

## Article

# An Experimental Study on Estimation of the Lateral Earth Pressure Coefficient (K) from Shaft Friction Resistance of Model Piles under Axial Load

Huseyin Suha Aksoy<sup>1</sup>, Nichirvan Ramadhan Taher<sup>1</sup>, Aykut Ozpolat<sup>2,\*</sup> , Mesut Gör<sup>1</sup>   
and Omer Muhammad Edan<sup>1</sup>

<sup>1</sup> Department of Civil Engineering, Engineering Faculty, Firat University, 23100 Elazig, Turkey; saksoy@firat.edu.tr (H.S.A.); taher.nichirvan@gmail.com (N.R.T.); mgor@firat.edu.tr (M.G.); omer.edan@gmail.com (O.M.E.)

<sup>2</sup> Department of Civil Engineering, Technology Faculty, Firat University, 23100 Elazig, Turkey

\* Correspondence: aozpolat@firat.edu.tr

**Abstract:** Estimating a pile shaft's frictional capacity is challenging and has been a controversial subject among researchers. In this study, the shaft friction resistance of non-displacement (pre-installed) model piles under axial load was investigated. Four different model piles were used, including steel, timber, and two composite piles (FRP and PVC filled with concrete). The angle of interface friction ( $\delta$ ) between test sand, and pile materials was determined using an interface shear test (IST) at four relative densities. Axial pile load experiments were implemented in a soil tank and piles were embedded into loose to very dense sand. Model pile load tests were performed in such a way that there was no end (point) bearing capacity (only friction was generated), and lateral friction resistance between the pile material and the soil along the pile shaft formed the complete bearing capacity of the model pile. According to experimental results, it was observed that, with increasing sand relative density and surface roughness of the pile material, the shaft friction resistance of the model pile increases. A back-calculation analysis was also performed to find the values of lateral earth pressure coefficient (K) using Burland's (1973) equation with the help of measured shaft friction capacity of the model pile load test. By performing multivariate regression analysis, an equation was obtained between the back-calculated lateral earth pressure coefficient (K) and other parameters. The obtained equation was used to calculate the K values given in other studies in the literature. It was determined that the obtained equation was in good agreement with the data in other studies. This equation can be beneficial in practice and can be advantageous for further study in the future.

**Keywords:** shaft friction resistance; lateral earth pressure coefficient (K); interface friction angle ( $\delta$ ); relative density ( $D_r$ ); interface shear test (IST)



check for  
updates

**Citation:** Aksoy, H.S.; Taher, N.R.; Ozpolat, A.; Gör, M.; Edan, O.M. An Experimental Study on Estimation of the Lateral Earth Pressure Coefficient (K) from Shaft Friction Resistance of Model Piles under Axial Load. *Appl. Sci.* **2023**, *13*, 9355. <https://doi.org/10.3390/app13169355>

Academic Editor: Tiago Miranda

Received: 10 July 2023

Revised: 2 August 2023

Accepted: 9 August 2023

Published: 17 August 2023



**Copyright:** © 2023 by the authors. Licensee MDPI, Basel, Switzerland. This article is an open access article distributed under the terms and conditions of the Creative Commons Attribution (CC BY) license (<https://creativecommons.org/licenses/by/4.0/>).

## 1. Introduction

Unlike shallow foundations, the load transfer mechanism through the pile to the soil layers is more sophisticated [1]. Generally, the end (point) bearing and skin friction are the two mechanisms that transfer the normal loads on piles into the soil. In some cases, such as weak soil deposits, the pile foundation system may be the only reliable system for transmitting the structural load to the ground. When there is no rock or stiff soil layer at a reasonable depth, the pile's end (point) bearing capacity is comparatively small and much of the resistance is caused by lateral friction or adhesion between the materials of the pile and the surrounding soil around the pile shaft.

Estimating the frictional capacity of the pile shaft is difficult and has been a matter of long discussions because there is great uncertainty about parameters related to soil and soil-pile interaction. Usually, there are two common methods in practice for prediction the shaft resistance of axially loaded piles: (1) estimating the pile-soil load transfer mechanism with

empirical relations [2–6] and (2) using finite element method analysis [7–13]. In practice, the ultimate pile shaft friction resistance in cohesionless soil can be calculated from the following equation, which was proposed by Burland [14].

$$Q_f = f_s \cdot P \cdot L = K \cdot \sigma'_v \cdot \tan \delta' \cdot P \cdot L \quad (1)$$

where  $f_s$  is unit skin friction,  $K$  is lateral earth pressure coefficient,  $\sigma'_v$  is an average vertical effective overburden pressure,  $\delta'$  is effective skin friction angle between soil and pile materials,  $P$  is the perimeter of the pile, and  $L$  is the embedded length of the pile. The ( $K$ ) value is considered the most difficult factor to estimate in Equation (1) [15]. Several researchers have attempted to estimate the  $K$  value from a retrospective analysis of field pile load tests, small-scale model pile load tests in the laboratory, and finite element analysis. Due to the large number of suggested  $K$  values equations, the estimated pile shaft resistance may differ by several hundred percent. Meyerhof and Adams [16] reported that the  $K$  value is a function of the internal friction angle of soil. The American Petroleum Institute's RP2A code [17] recommended that the  $K$  value of 0.8 to 1 be used for estimating shaft friction resistance of driven piles with open and closed ends in sand. However, it does not take into account whether the pile is in compression or tension. In addition, some studies have uncovered the restrictions of the API code design instructions for tension piles, and new design methods have been proposed [18–20]. Alawneh [5] stated that the value of  $K$  ranges widely between Rankine's active earth pressure coefficient ( $K_a$ ) and passive earth pressure coefficient ( $K_p$ ), in some cases, maybe greater than  $K_p$ . He also asserted that the maximum  $K$  value is a function of the relative density of sand, pile diameter, and initial stress condition. Jazebi and Ahmadi [21], using finite element methods, indicated that the  $K$  value is approximately equal to earth pressure coefficient at rest ( $K_0$ ) for non-displacement piles.

When estimating the friction capacity of piles, the interface friction angle ( $\delta$ ) between the soil and the pile materials is crucial. The interface friction between sand and other construction materials has been the subject of several investigations in the past. To this end, In the literature, a wide range of geotechnical laboratory experiments have been employed, such as a direct shear test, large-scale shear box test, and ring torsion apparatus. Factors that influence the interface friction angle ( $\delta$ ) have been stated in the literature as internal friction angle of soil ( $\phi$ ), moisture content, soil density, soil type, the surface roughness of the material, soil particle shapes (angular or round), relative roughness (surface roughness of the material divided by soil particle mean diameter ( $D_{50}$ )), percentage of coarse grains, the levels of normal stress, soil, and shearing rate [22–36].

Researchers attempted to conduct small- and large-scale model pile load experiments to better understand the behavior of shaft friction capacity of non-displacement (bored or drilled shaft) piles due to the high expense of full-scale pile load studies. The mobilized unit shaft resistance of the bored pile in sand is usually influenced by some factors such as the initial relative density of sand and stress state [37–39], the roughness between soil and pile material [40–44]. The surface roughness of a pile is usually introduced as a normalized roughness ratio ( $R_n = R_t/D_{50}$ ), where  $R_t$  is the maximum surface profile height, and  $D_{50}$  is the mean particle size diameter of the soil mass, as shown in Figure 1 [9,40]. Salgado et al. [45] employed a calibration chamber test and two-dimensional finite element analysis using a two-surface-plasticity constitutive model to examine the behavior of bored pile under axial load in sand. It was discovered that the ultimate unit shaft resistance is considerably influenced by the  $K$  value and the relative density of soil. Additionally, they demonstrated that in comparable circumstances, a small-size model pile produces far more unit shaft resistance than a full-scale pile.

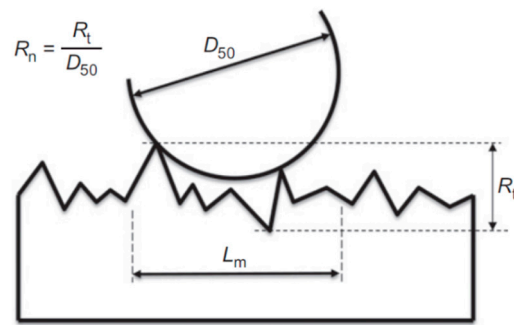


**Figure 1.** Description of the maximum roughness  $R_t$  and the normalized roughness  $R_n$  [9].

Due to the high degree of soil parameter uncertainty and the intricate pile–soil load transmission process, estimating the shaft frictional resistance of piles has been a controversial subject among researchers until now. Very little research has been carried out in the literature on shaft resistance of full-scale model piles under axial load in sand [43]. Most of the studies have used small-scale steel model piles under tensile load experimentally to back-calculate the  $K$  value from the friction capacity of the pile shaft [46–48]. Research dealing with shaft friction resistance of timber and composite model piles (concrete-filled FRP and PVC) under axial load in the sand was not encountered.

The purpose of this study is to examine the shaft friction resistance of four different non-displacements (pre-installed) model piles embedded in sand, including closed-end steel pipe piles, timber piles and two composite piles (FRP and PVC filled with concrete). At different relative densities, the test sand's internal friction angle was found by conducting a series of shear box experiments. The interface friction angle between sand and pile material was determined using an interface shear test (IST). In addition, a surface roughness test was carried out to obtain the maximum surface roughness of all model piles. Model pile tests were executed under axial load in such a method that the end (point) bearing of the pile does not exist, and the whole pile capacity was produced from lateral friction resistance between the pile shaft and the neighbouring soil. Additionally, it aims to determine how the relative density of sand affects the shaft resistance of non-displacement piles and back-calculate the  $K$  value using the results of model pile load tests.

## 2. Materials and Method

The characteristics of friction should be established in order to calculate the shaft friction capacity of single piles. For this reason, the internal friction angle of sand for different relative densities, the surface roughness of the pile materials and interface friction angles between sand and pile materials were determined. After that, pile model load tests were carried out in the laboratory to find the maximum frictional resistance for each mode pile at different relative densities.

### 2.1. Test Sand

River sand with a uniform gradation was utilized in this study. Sand has been cleaned, dried in an oven, sieved using sieve #18 (1 mm), and retained on sieve #200 (0.075 mm), as done by previous studies [20,49]. To see the geometry and colour of sand particles, a zoomed-in photo was taken by the digital camera Figure 2, it appeared that sand particles are mostly dark in colour and have angular to sub-angular shapes. The angle of repose of sand was found to be  $35^\circ$  measured in accordance with ASTM- C1444-00 [50], Figure 3. Sieve analysis was conducted to obtain the particle distribution curve of test sand in accordance with ASTM D422-63 [51], Figure 4. The specific gravity of sand was determined based on ASTM D854-14 [52]. The maximum and the minimum dry densities for sand were measured by experiment in agreement with ASTM D4254 [53]. The measured index parameters of sand are listed in Table 1.



Figure 2. Photo of the geometry and colour of sand particles.

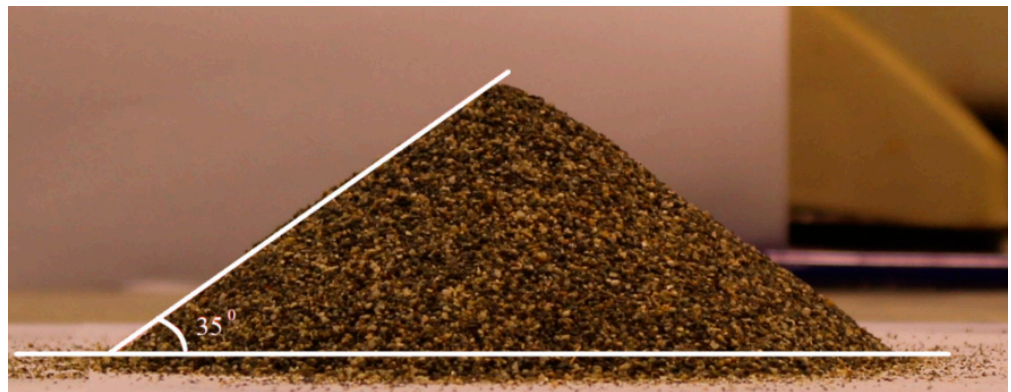


Figure 3. The angle of repose of sand.

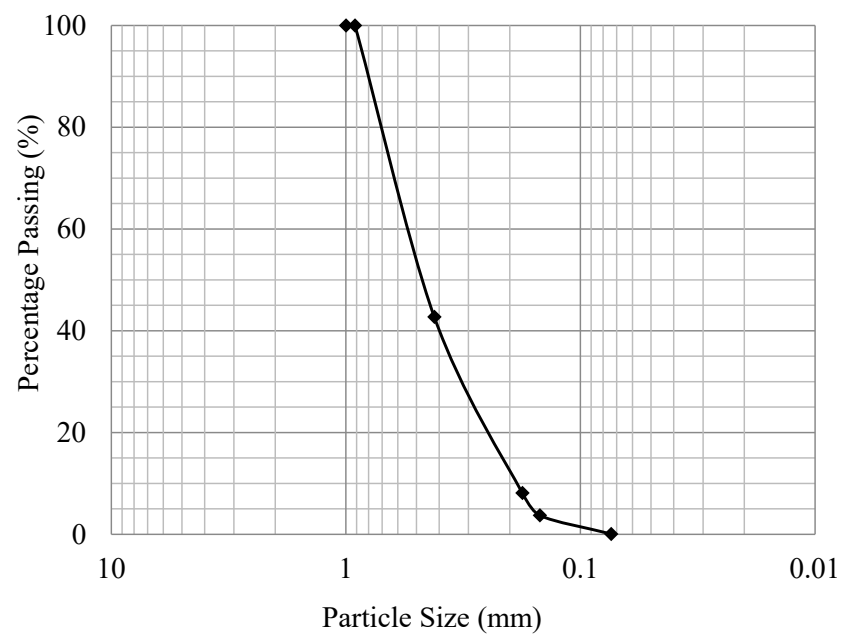


Figure 4. The grain size distribution curve of sand.

**Table 1.** Physical properties of sand used in the study.

Property	Value
D <sub>50</sub> , (mm)	0.475
Uniformity Coefficient, (C <sub>u</sub> )	2.895
Curvature coefficient, (C <sub>c</sub> )	0.980
USCS Classification	SP
Specific gravity, (G <sub>s</sub> )	2.77
γ <sub>dmax</sub> , (kN/m <sup>3</sup> )	17.66
γ <sub>dmin</sub> , (kN/m <sup>3</sup> )	14.32
Maximum void ratio (e <sub>max</sub> )	0.898
Minimum void ratio (e <sub>min</sub> )	0.539
Maximum – Minimum grain size, (D <sub>max</sub> – D <sub>min</sub> ) (mm)	1 – 0.074

## 2.2. Model Piles and Sand Tank

In model tests, the dimensions of the test tank should be determined so that the boundary effects will have the least effect on the test results. In the literature, many studies have been carried out on the selection of the dimensions of the pile and the test tank in order to ensure semi-infinite medium conditions where the boundary effects do not change the experimental results. As a result of these studies, if there is a 2B (B is the dimension of the foundation) gap between the edge points of the pile and the tank sides, the boundary conditions will not affect the test, and thus, semi-infinite conditions will be provided [54–56]. In this study, the diameter of the pile was determined as 5 cm since the side length of the experiment tank was 75 cm in order to provide semi-infinite conditions.

Due to the stress-dependent soil properties, it is important to accurately model the prototype stress conditions in small-scale modeling experiments. One of the common ways to apply gravity (g) in model experiments is re-establish full-size stress levels. Details of the rules and modeling practices used in laboratory modeling can be found in [57]. Information about the scaling laws used in this study is given in Table 2.

**Table 2.** Scaling Laws.

Physical Parameters	Scaling Factor (Model/Prototype)
Gravity (m/s <sup>2</sup> )	1
Force (N)	1/n <sup>3</sup>
Length (m)	1/n
Displacement (m)	1/n <sup>2-α</sup>
Area (m <sup>2</sup> )	1/n <sup>2</sup>
Stiffness (N)	1/n <sup>α</sup>
Strain	1/n <sup>1-α</sup>
Density (kg/m <sup>3</sup> )	1
Stress (kPa)	1/n
α	1

In this study, an in-plane strain condition of the test system is assumed. The dimensions of the test system and the pile are similar in all experiments. While the pile diameter was 50 mm (The equivalent in the prototype was 1 m), the thickness of the soil layer was constant and 900 mm (The equivalent in the prototype was 18 m). The width of the system was 750 mm (The equivalent in the prototype was 15 m), according to the scaling law given in Table 3.

**Table 3.** Physical and chemical properties of model piles.

Properties	Steel	Wood	FRP	PVC	Unit
Density	78.5	5.5	19.60	5.90–13.30	kN/m <sup>3</sup>
Elasticity modulus	210,000	12,600	15,700	1800–2410	Mpa
Flexutural modulus	16,400–106,000	8550	10,000	1520–2540	Mpa
Ultimate Tensile strength	360–510	5.24	160	9.00–53.8	Mpa
Yield strength	300	31	300–1000	30.0–65.0	Mpa
Shear strength	230	8.34	35–300	0.460–5.01	Mpa

In this study, four model piles with different materials were used, including closed-end steel pipe piles, timber piles, concrete-filled PVC and FRP pipe piles. The diameter and length of the test piles were 50 mm and 600 mm, respectively, and the pile was 500 mm embedded into the sand during the test. Plain concrete with a compressive strength of 16 MPa was used to fill the FRP and PVC pipe piles because examining the model piles' shaft friction resistance is the primary goal of the study. The steel pile and the timber pile were both constructed using St-37 steel and beech tree, respectively, a 50% fiberglass-included FRP pipe was used as the FRP pile, and PVC-U type cylindrical profile was used as the PVC pile. The four model piles used in this study are depicted in Figure 5. Since the main objective of this study is to investigate the friction capacity of model piles, therefore four different materials were selected to study their friction capacity when used as pile foundations. In pile foundations, different construction materials offer unique advantages. Steel piles are favored for their high strength, allowing them to bear heavy loads in deep foundation applications such as tall buildings and bridges. Timber piles are suitable for smaller structures due to their ease of installation and cost-effectiveness, making them a viable option for residential and light commercial projects. FRP (Fiber-Reinforced Polymer) filled-with-concrete piles excel in corrosive environments, as they are resistant to chemical degradation, making them valuable in marine and industrial settings. PVC filled-with-concrete piles provide enhanced resistance to weathering and groundwater corrosion, making them a durable choice for foundations in certain environmental conditions. The selection of the most advantageous material for pile foundations depends on factors such as the project's scale, load requirements, site conditions, and long-term performance considerations [58–60]. The mechanical and physical properties of model piles are listed in Table 3. The 3D schematic diagram of the soil tank is as seen in Figure 6.



**Figure 5.** Model piles.

Four different relative densities employed in this investigation were obtained using a hand compactor. Vibration equipment is generally used for compaction of sand [61]. Relative density experiments were performed in the laboratory; the different relative densities used in this study are ( $D_r = 10\%$ ,  $40\%$ ,  $65\%$  and  $90\%$ ). The summary of obtaining various relative densities of sand with the compaction technique corresponding to the dry unit weights and the void ratio is presented in Table 4. The water content measured under laboratory conditions is about 1%. Compaction process tests were carried out at this water content, and then the dry unit weight was calculated. To ensure the homogeneity of the sand in the soil tank during the tests, small cans were positioned in various areas within the soil tank to control the relative density of the sand. After each test, the small cans were carefully extracted from the soil tank and the density of the sample was calculated, as has been performed in the literature [62].

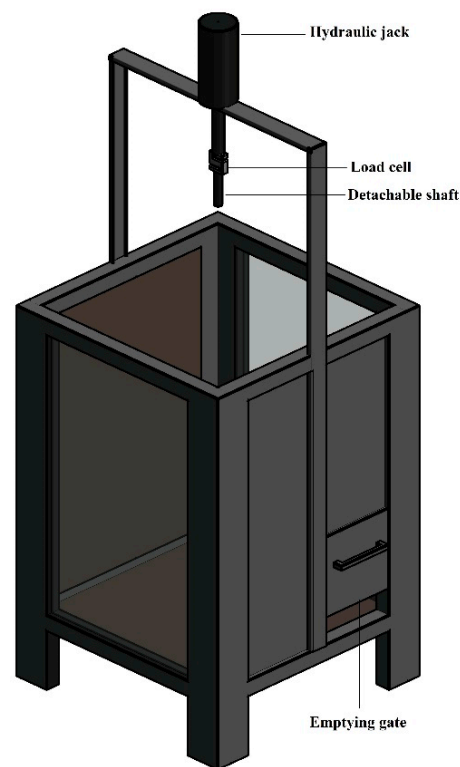


Figure 6. 3D Schematic diagram of the soil tank.

Table 4. Void ratio, compaction method, and dry unit weights of test sand corresponding to different relative densities.

Relative Density ( $D_r$ ), (%)	Average Dry Unit Weight ( $\gamma_d$ ), ( $\text{kN/m}^3$ )	Void Ratio ( $e$ )	Compaction Process
10	14.6	0.86	From a height of 10 to 15 cm, test sand was poured until the model tank was filled to the necessary depth.
40	15.5	0.75	The test sand was poured from a height of 5–10 cm and the tank was filled with layers every 10 cm, each point (15 cm $\times$ 15 cm) was compacted for less than a second (for a moment).
65	16.3	0.66	The test sand was poured from a height of 5–10 cm and the tank was filled with layers every 10 cm, each point (15 cm $\times$ 15 cm) was compacted for two seconds.
90	17.3	0.57	The test sand was poured from a height of 5–10 cm and the tank was filled with layers every 5 cm, each point (15 cm $\times$ 15 cm) was compacted for eight seconds.

### 2.3. Interface Shear Test

For each relative density, the internal friction angle ( $\phi$ ) of the sand and the interface friction angle ( $\delta$ ) between the sand and the pile materials were measured using the shear box test (6 cm  $\times$  6 cm  $\times$  2 cm). To determine the angle of internal friction ( $\phi$ ) of sand at different relative densities, a shear box test was performed in accordance with ASTM D-3080 [63]. Interface friction tests were performed according to ASTM D5321/D5321M-17 [64] to find the interface friction angle ( $\delta$ ) in-between sand and different pile materials at four different relative densities. The internal friction angle of sand and the interface friction angle between sand and model pile materials, which correspond to different relative densities, are summarized in Table 5. As can be observed, the angle of internal friction increases as relative density does as well. The interface friction angle also increases with

increasing relative density, but it begins to decrease under very dense conditions, such as at 90% relative density. This behavior has also been observed in previous research [22,32,65]. It can be seen that the internal friction angle of sand for different relative densities is quite high due to the shape of the sand particles. The shape of the sand particles has a considerable effect on the angle of internal friction. The sand with high internal friction angle was also observed by Stark et al. [66].

**Table 5.** Internal friction angle of sand ( $\phi$ ) and interface friction angles ( $\delta$ ) between sand and pile materials versus relative density.

$D_r$ (%)	$(\phi)$ (°)	$(\delta)$ of Sand-Timber (°)	$(\delta)$ of Sand-PVC (°)	$(\delta)$ of Sand-FRP (°)	$(\delta)$ of Sand-Steel Material (°)
10	41.0	35.1	26.1	23.7	20.0
40	44.3	36.2	28.7	26.2	21.0
65	48.7	37.9	31.4	28.3	22.5
90	52.4	35.3	30.3	28.2	21.0

**2.4. Surface Roughness of Model Piles**

The pile surface’s roughness has been known as one of the most significant factors that impact the mobilized shaft resistance of the pile. The surface roughness of the model piles was measured by the Mutitoyo SJ-201 surface roughness device. By using maximum roughness of the materials, normalized surface roughness was calculated as stated in Basu et al. [9]. Figure 7 defines the parameters of surface roughness, and the calculated roughness parameters of all model piles are listed in Table 6.

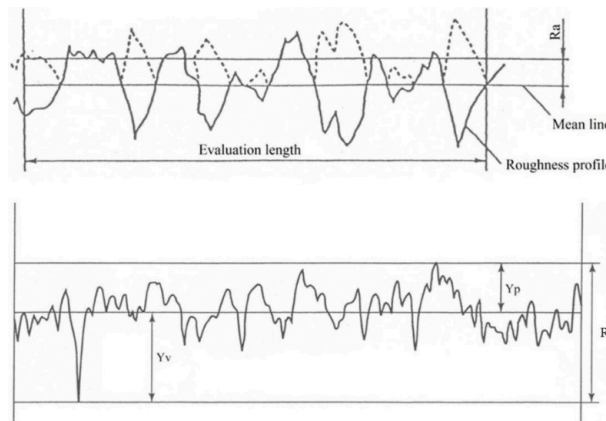


**Figure 7.** Description of mean line roughness  $R_a$  and maximum roughness  $R_t$ .

**Table 6.** Table roughness parameters of the model piles used in this study.

Model Pile	Arithmetic Mean Surface Roughness, $R_a$ , ( $\mu\text{m}$ )	Maximum Surface Roughness, $R_t$ , ( $\mu\text{m}$ )	$D_{50}$ , ( $\mu\text{m}$ )	Normalized Surface Roughness, $(R_t/D_{50})$ , $R_n$ , ( $\mu\text{m}$ )
Timber	4.17	24.45	475	0.051
PVC	1.78	12.83	475	0.027
FRP	1.63	8.84	475	0.019
Steel	0.55	3.43	475	0.007

**2.5. Model Pile Installation Method and Test Procedure**

Model pile tests were conducted under axial load in such a manner that the end (point) bearing capacity of the pile does not exist, and the whole pile capacity was derived by the lateral friction resistance between the pile material and sand along the pile shaft. For this purpose, a Styrofoam with dimensions (12 cm  $\times$  12 cm  $\times$  10 cm) was used. A hole with a diameter of 5.1 cm was cut out of the middle of the Styrofoam body to ensure there was

enough space between the edges of the pile and the Styrofoam during the load test, as illustrated in Figure 8a.

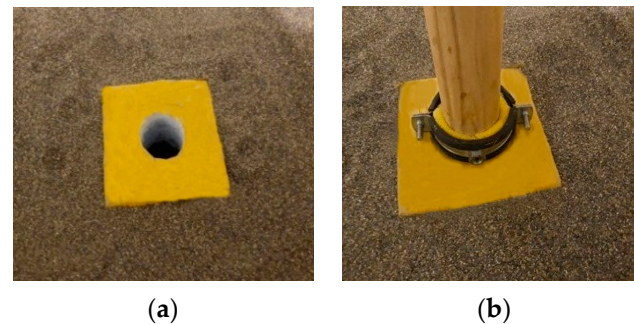


**Figure 8.** (a) Styrofoam with the hole, (b) sponge strip wrapped around the pile bottom by using a clamp.

In order to install model piles, a specific kind of epoxy adhesive was used to fix the pile to a detachable shaft, which was then threaded into a load cell. The soil tank was filled with sand for each test to a depth of 30 cm, and then, a Styrofoam body was put in the middle of the soil tank, after which an additional 10 cm of sand was filled to stabilize the Styrofoam body. After that, the model pile with a detachable shaft threaded into a load cell was lowered using a hydraulic jack until the bottom of the pile protruded 2 cm into the pre-drilled hole inside the Styrofoam. Following that, a clamp was used to wrap a sponge strip around the pile bottom. To stop sand particles from leaking into the hole as illustrated in Figure 8b, the tank was filled to the depth of 90 cm. Because the model piles have been pre-installed, they are considered non-displacement (bored) piles because they do not displace the soil Salgado et al. [45]. A total of sixteen model pile load tests were performed in the soil model tank, four load tests for each pile with sand relative densities (10%, 40%, 65% and 90%).

Using a hydraulic jack, the axial load was applied to the single model pile, and the two LVDTs were used for measuring pile displacement; the vertical displacement rate of the model pile was 1 mm/min. The loading machine was computer controlled, and all data from LVDTs and load cells were recorded. A two-dimensional schematic diagram of the sand tank, test setup, and experimental apparatus can be seen in Figure 9.

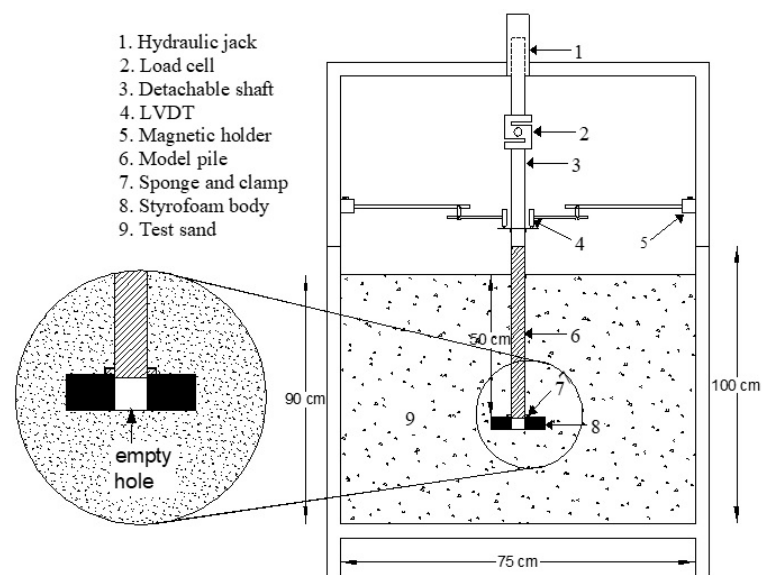


**Figure 9.** Schematic diagram of the test setup for a typical shaft friction test.

### 3. Results and Discussion

#### 3.1. Experimental Results

A total of 16 model pile shaft friction tests were performed under axial compressive load in this study. Four different model piles were used and embedded into loose to very dense sand. The results were obtained in terms of load–displacement curves, as shown in Figure 10. From the load–displacement curves of the model piles, it is evident that as the relative density of sand increases, so does the shaft friction resistance of model piles. Among the model piles, it can be seen that the timber pile has the highest ultimate shaft resistance while the steel one has the lowest; this indicates that the surface roughness has a great effect on the shaft resistance of the pile. Moreover, it is clear from the load–displacement curves that the model piles' maximum shaft friction resistance is mobilized when the displacement reaches around 5–10% of the diameter of the pile. Many researchers indicated that the shaft friction resistance of the full-scale piles is mobilized when the pile displacement is in the range of 0.5–1% of the pile diameter [7,21,67]. Research performed on model pile load tests indicates that The displacement needed to mobilize the ultimate shaft friction resistance is between 5 and 10% of the pile [37,68]. In this study, the ultimate shaft friction resistance of the model piles was selected based on the criterion that the displacement of the pile is 5% of the pile diameter. The variation in the ultimate shaft resistance of model piles versus relative density is illustrated in Figure 11.

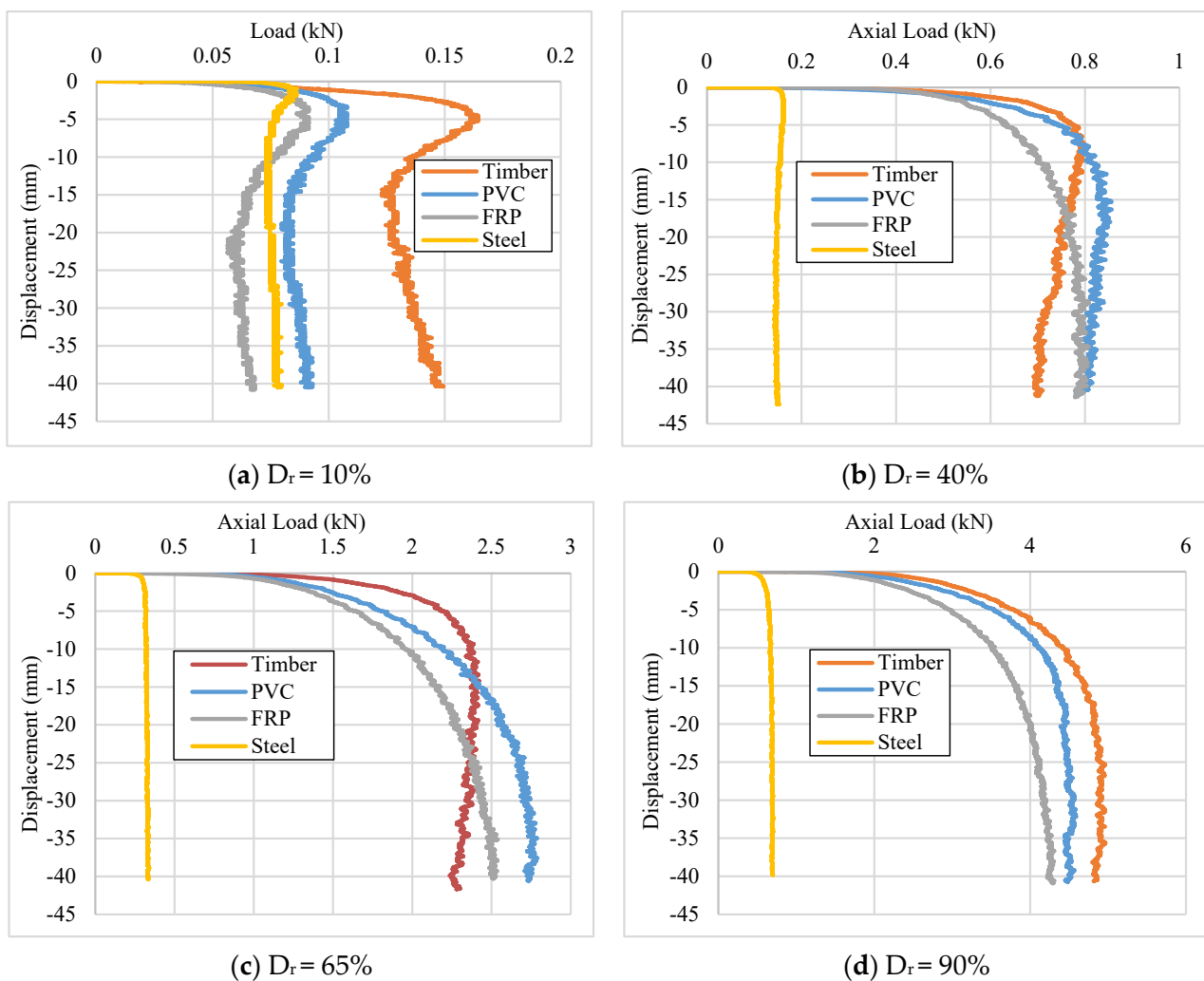


Figure 10. Load–displacement curves of model piles in different relative densities.

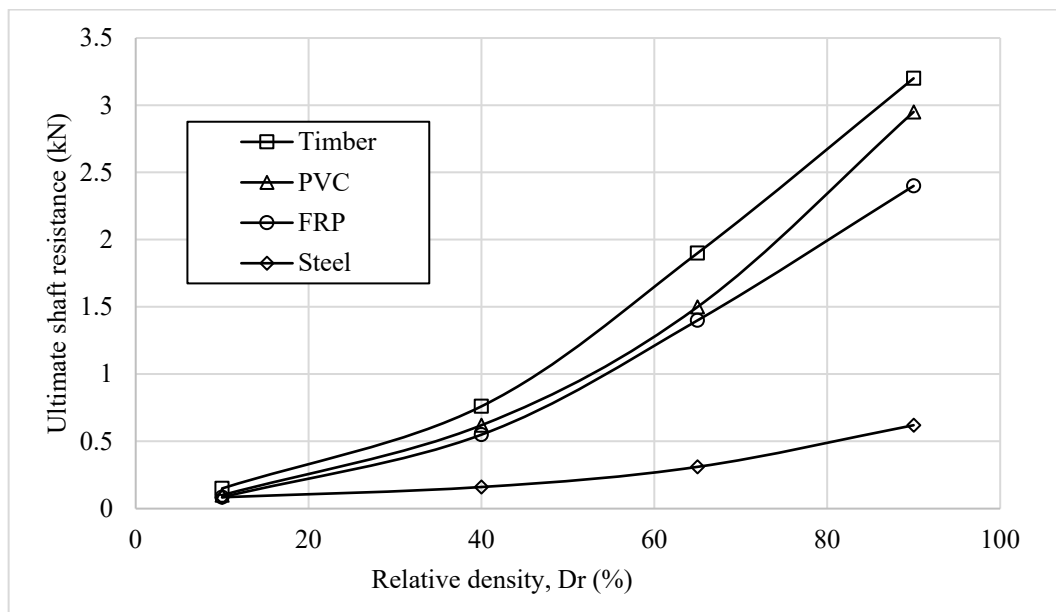


Figure 11. Variation of the maximum resistance of model shaft piles versus relative density of sand.

3.2. Back-Calculation of K Values from Experimental Results

The values of the lateral earth pressure coefficient, K, are also back-calculated from Equations (1) and (2) as follows, and the results listed in Table 7.

$$K = \frac{Q_f}{\sigma'_v \cdot \tan \delta' \cdot P.L} \tag{2}$$

Table 7. Back-calculated K values.

Model Pile	Dr (%)	$\gamma_d$ (kN/m <sup>3</sup> )	$Q_f$ (kN)	$\sigma'_v$ (kN/m <sup>3</sup> )	( $\delta$ ) (°)	K
Timber	10	14.6	0.15	3.650	35.1	0.74
	40	15.5	0.76	3.875	36.2	3.41
	65	16.3	1.90	4.075	37.9	7.63
	90	17.3	3.20	4.325	35.3	13.31
PVC	10	14.6	0.10	3.650	26.1	0.71
	40	15.5	0.62	3.875	28.7	3.72
	65	16.3	1.50	4.075	31.4	7.68
	90	17.3	2.95	4.325	30.3	14.86
FRP	10	14.6	0.08	3.650	23.7	0.67
	40	15.5	0.55	3.875	26.2	3.67
	65	16.3	1.40	4.075	28.3	8.12
	90	17.3	2.40	4.325	28.2	13.18
Steel	10	14.6	0.05	3.650	20.0	0.52
	40	15.5	0.16	3.875	21.0	1.37
	65	16.3	0.31	4.075	22.5	2.34
	90	17.3	0.62	4.325	21.0	4.75

It can be seen that the K values are different for each material at the same relative density, and this is because each material has different surface roughness; the material with higher surface roughness has higher K values. The back-calculated K values vary from 0.52 to 14.86, and it is obvious that the K values obtained are quite high and all are greater than  $K_A$  and some values are even greater than  $K_P$ , especially in high relative density for PVC, timber and FRP model piles. As reported by [37,46], the K value can be greater than  $K_P$  in some situations. In addition, sand particles used in this study are of small size and angular shape, as stated by Han et al. [33]; this causes high friction resistance between the pile shaft and sand and, consequently, high K values are obtained. Another reason

is that small-scale model piles generate considerably higher shaft friction resistance than full-scale piles [45]. The test sand has a high internal friction angle, and all of the model pile materials, with the exception of steel, have high interface friction angles with the sand; therefore, there is a potential for sand to dilate mostly in high relative density, this, of course, makes a contribution to the K values measured [69].

From Figure 10, it can be seen that the timber model pile has the highest shaft friction resistance at 90% relative density, while the maximum K value belongs to the PVC model pile; this is because PVC is a soft material and has a lower surface hardness compared to the timber, that is why during loading, sand particles try to scratch the surface of the PVC pile and form high friction resistance. In addition, the skin friction angle ( $\delta$ ) between sand-PVC materials is lower than sand-timber and it is inversely proportional to the tangent of the skin friction angle, as shown in Equation (2).

### 3.3. Shaft Friction Resistance and K Values of Model Piles at Different Relative Densities

Figures 12 and 13 show the increase in maximum shaft friction resistance of model piles and back-calculated K values in different relative densities, respectively. Obviously, the increase in shaft friction resistance and K value with increasing relative sand density for a model pile with a smooth surface is less than for a model pile with a rough surface. For example, the ultimate shaft friction resistance and K value of the steel model pile at 90% relative density are about 11 and 10 times greater than 10% relative density, respectively, while for timber model pile, they are about 21 and 18 times. However, the FRP and PVC model piles have lower surface roughness than timber model pile but the increase in ultimate shaft friction resistance and K values of FRP and PVC model piles with the increasing relative density of sand are greater than the timber model pile. For instance, the ultimate shaft friction resistance and K value of the PVC model pile at 90% relative density are about 29 and 21 times greater than 10% relative density, respectively. The reason is that the PVC and FRP model piles are soft materials and have a lower hardness than steel and timber model piles; that is why with the high relative density of sand, sand can dilate more and sand particles try to scrape the surface of the model piles and produces more friction resistance than low relative density.

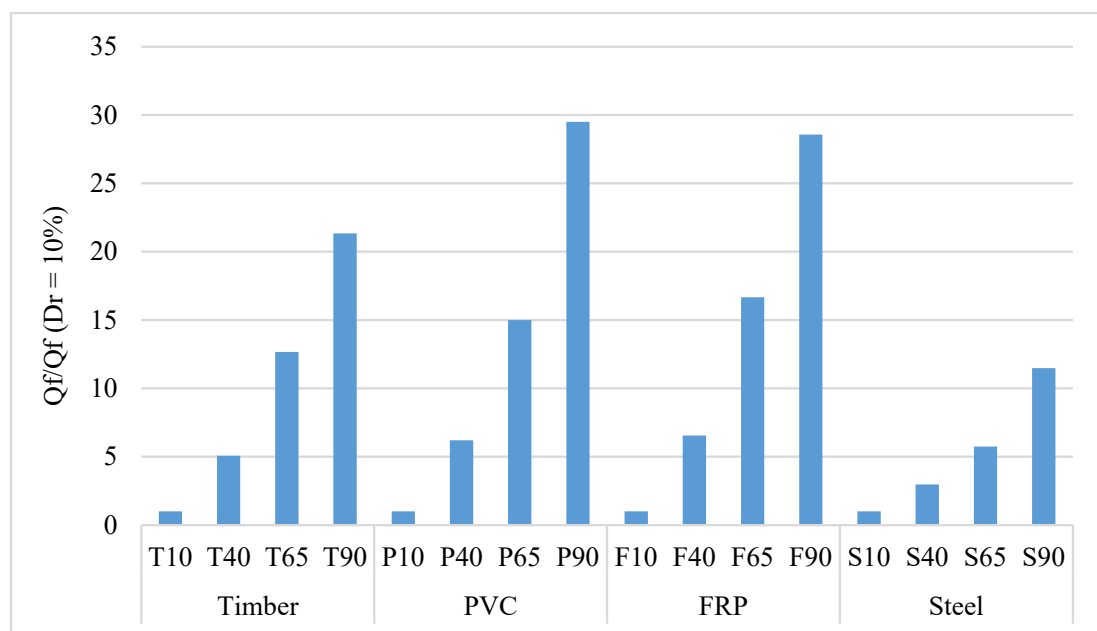


**Figure 12.** The increase in the ultimate shaft friction resistance of model piles at different relative densities.

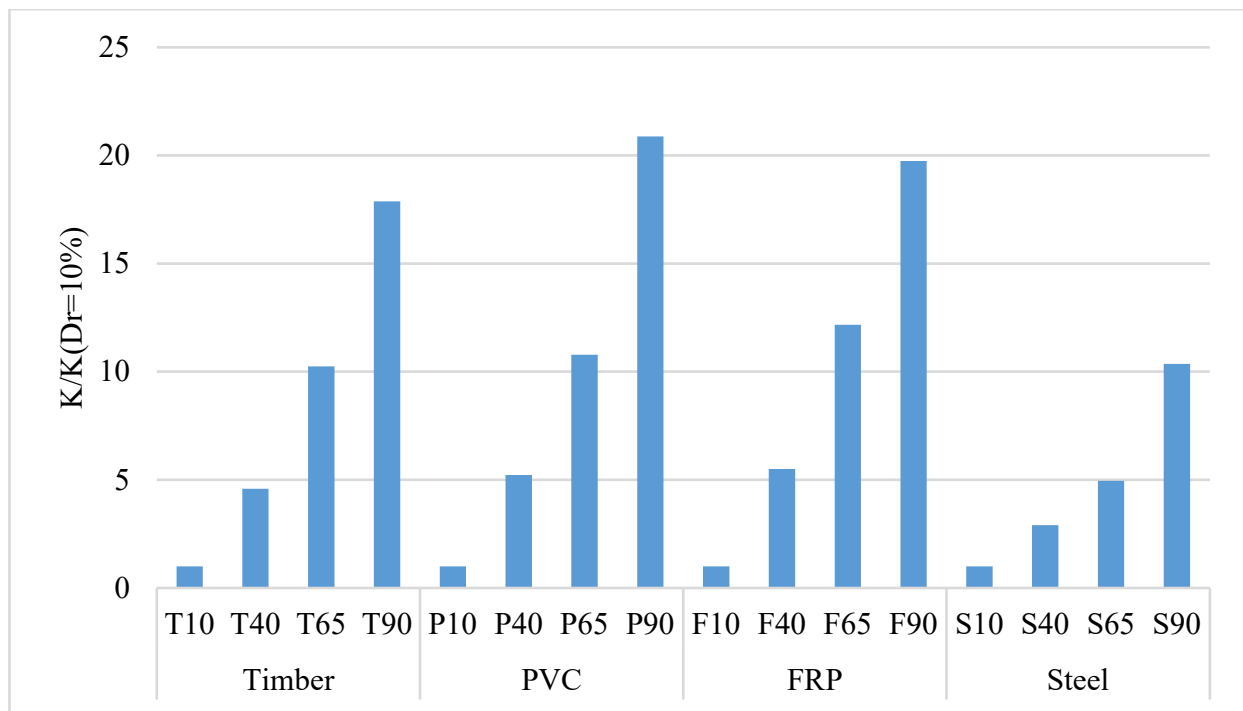


Figure 13. The increase in the K value of model piles at different relative densities.

3.4. Statistical Analysis for Estimation of K Values

Nonlinear statistical analysis was carried out for the prediction of the K values. Some experimental data from the work performed by Alawneh et al. [70] were also used in the multiple nonlinear regression analysis. Many correlations of K values were tried, but using the results of this study, the best coefficient of determination was obtained with  $R^2 = 0.96$ , while including the results of Alawneh et al. [70], the coefficient of determination was obtained with  $R^2 = 0.95$  (Table 8).

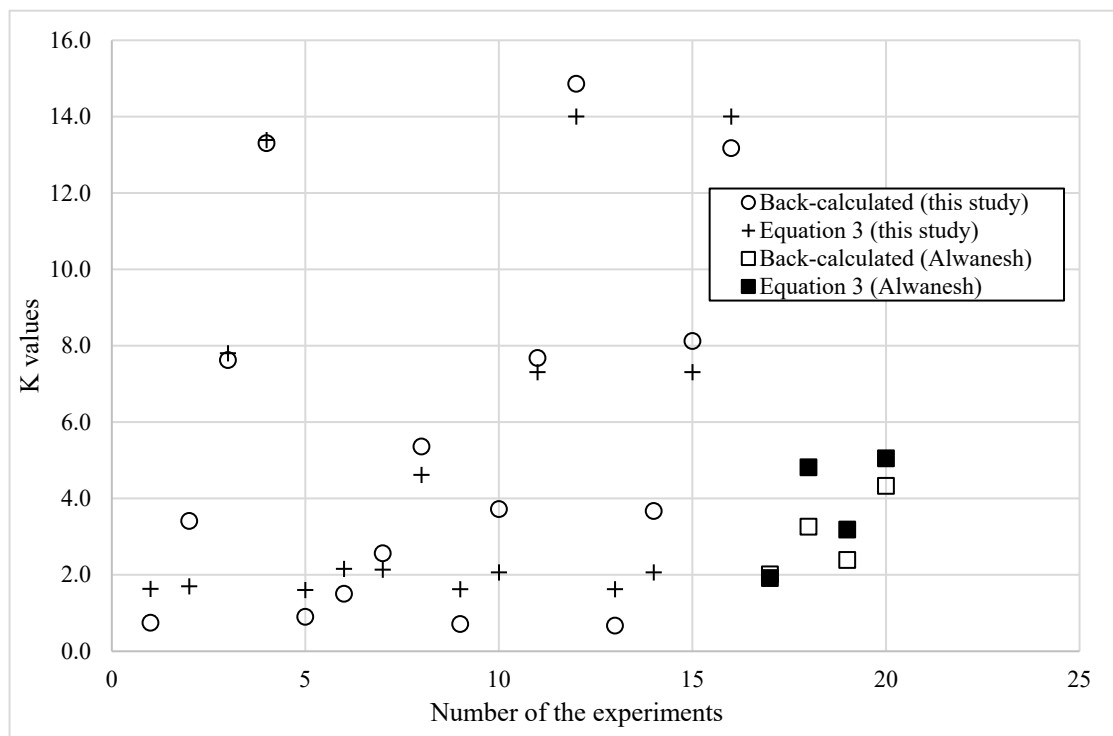
Table 8. In the research of Alawneh [37].

Model Pile	Dr (%)	$\gamma_n$ (kN/m <sup>3</sup> )	$Q_f$ (kN)	$\sigma'_v$ (kN/m <sup>3</sup> )	( $\delta$ ) (°)	K
	45	15.2	0.15	3.650	35.1	2.01
	70	16.4	0.76	3.875	36.2	3.26
	40	15.2	1.90	4.075	37.9	2.39
	70	16.4	3.20	4.325	35.3	4.33

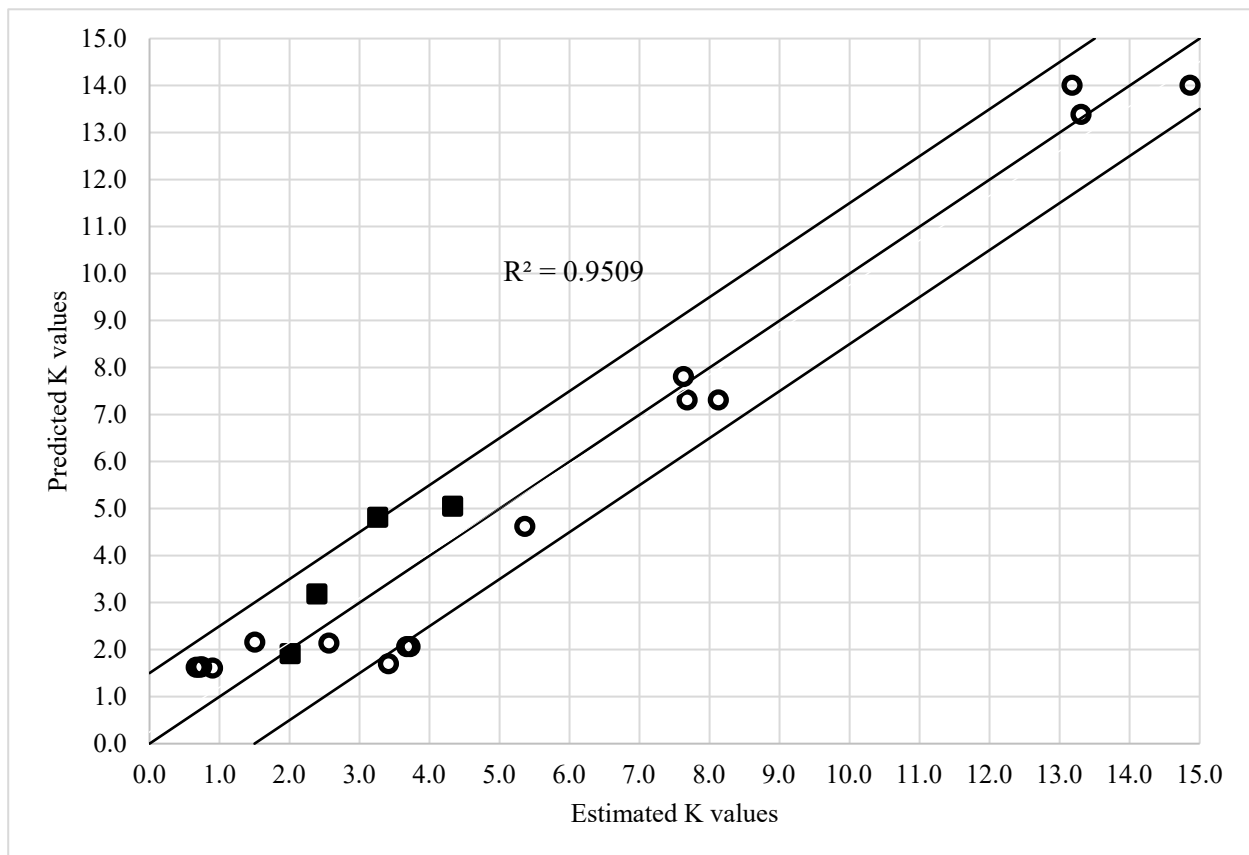
The correlation obtained as a result of the statistical analysis is given in Equation (3). The K values calculated from the experimental results and the predicted K values are compared in Figure 14.

$$K = e^{(A \cdot Dr + B \cdot \gamma + C \cdot \phi + D \cdot \delta^{0.05} + E \cdot \sigma'_v + F \cdot R_n + G) + H} \tag{3}$$

where Dr is the relative density of sand,  $\gamma$  is unit weight,  $\phi$  is the internal friction angle of sand,  $\delta$  is the skin friction angle,  $\sigma'_v$  is the average vertical overburden pressure,  $R_n$  is the normalized roughness coefficient, and A, B, C, D, E, F are coefficients of the equation, which are given in Table 9.



(a)



(b)

**Figure 14.** (a,b) comparison between the calculated K values from experimental results and predicted K values from Equation (3).

**Table 9.** Coefficients of Equation (3).

A	B	C	D	E	F	G	H
0.0639	0.1000	0.0324	−1.1846	11.2511	10.5987	−11.9945	1.5905

#### 4. Scale Effect and Limitation

In this study, the scale of the full-scale piles has been reduced while sand is the same as in the field. As a result, the small model piles may not perform the same role as the full-scale piles and may have an impact on the experimental results. This phenomenon is known as scale effects. Burland [14] stated that this phenomenon happens as a result of different stress levels experienced during field tests of prototype and experimental models. For this reason, we cannot only rely on the experimental results of small model piles to estimate the exact behaviour of full-scale piles. However, the results of the experimental tests can be used as a useful database to better understand the behaviour of full-scale friction piles using field load testing, numerical analysis, and centrifuge load test.

#### 5. Conclusions

In this study, a series of axial model pile load tests were executed to examine the shaft friction resistance of different model piles (different materials) embedded into loose to very dense sand. The model piles were installed as non-displacement (bored) piles. The lateral earth pressure coefficient was back-calculated from the experimental test results. Multiple nonlinear regression analysis was carried out, and a correlation was proposed for estimation of K values. Based on the experimental outcomes and statistical analysis, the following conclusions can be drawn.

- The shaft friction resistance of all model piles increases with increasing relative density in a nonlinear relationship. From the load–displacement curves, the ultimate shaft friction resistance of the model piles is mobilized when the pile displacement reaches approximately 5–10% of the pile diameter.
- The ultimate shaft friction resistance of the model piles is strongly affected by the surface roughness of the pile materials. This effect can be clearly observed between ultimate shaft resistance of timber and steel model piles. This indicates that the pile with high surface roughness develops the propensity of sand to dilate during axial loading, particularly at high relative density, which leads to an increase in lateral earth pressure against the pile surface.
- The maximum K value was obtained from the PVC model pile at 90% relative density. The reason is that due to the low surface hardness of PVC, sand particles try to scratch the surface of the PVC pile during loading, which results in high friction resistance values.
- From back-calculation of the lateral earth pressure coefficient by using experimental results and statistical analysis, the K value depends on the initial stress condition, the relative density of sand, internal friction angle of sand, the skin friction angle between sand and pile materials, and normalized roughness of the pile materials. A correlation was proposed for the estimation of K value, and good agreement was found between the predicted K values and calculated K values from the experimental results.

**Author Contributions:** Methodology, M.G. and O.M.E.; Formal analysis, N.R.T.; Writing—original draft, N.R.T.; Writing—review & editing, H.S.A., N.R.T. and A.O. All authors have read and agreed to the published version of the manuscript.

**Funding:** This study was funded by the Firat University Scientific Research Projects Coordination Unit (FUBAP) with the project number MF.18.39 and MF.18.42.

**Institutional Review Board Statement:** The study did not require ethical approval.

**Informed Consent Statement:** Not applicable.

**Data Availability Statement:** All data, models, and code generated or used during the study appear in the submitted article.

**Conflicts of Interest:** The authors declare no conflict of interest.

## References

1. Coduto, D.P.; Kitch, W.A.; Yeung, M.-C.R. *Foundation Design: Principles and Practices*; Prentice Hall: Upper Saddle River, NJ, USA, 2001.
2. Coyle, H.M.; Reese, L.C. Load transfer for axially loaded piles in clay. *J. Soil Mech. Found. Div.* **1966**, *92*, 1–26. [[CrossRef](#)]
3. Sulaiman, I.H.; Coyle, H.M. Uplift resistance of piles in sand. *J. Geotech. Eng. Div.* **1976**, *102*, 559–562. [[CrossRef](#)]
4. Randolph, M.F.; Wroth, C.P. Analysis of deformation of vertically loaded piles. *J. Geotech. Geoenviron. Eng.* **1978**, *104*, 1465–1488. [[CrossRef](#)]
5. Alawneh, A.S. Modelling load–displacement response of driven piles in cohesionless soils under tensile loading. *Comput. Geotech.* **2005**, *32*, 578–586. [[CrossRef](#)]
6. Goel, S.; Patra, N.R. Prediction of load displacement response of single piles under uplift load. *Geotech. Geol. Eng.* **2007**, *25*, 57. [[CrossRef](#)]
7. Loukidis, D.; Salgado, R. Analysis of the shaft resistance of non-displacement piles in sand. *Géotechnique* **2008**, *58*, 283–296. [[CrossRef](#)]
8. Lee, S.; Long, J.H. Skin friction features of drilled CIP piles in sand from pile segment analysis. *Int. J. Numer. Anal. Methods Geomech.* **2008**, *32*, 745–770. [[CrossRef](#)]
9. Basu, P.; Loukidis, D.; Prezzi, M.; Salgado, R. Analysis of shaft resistance of jacked piles in sands. *Int. J. Numer. Anal. Methods Geomech.* **2011**, *35*, 1605–1635. [[CrossRef](#)]
10. Lashkari, A. Prediction of the shaft resistance of nondisplacement piles in sand. *Int. J. Numer. Anal. Methods Geomech.* **2013**, *37*, 904–931. [[CrossRef](#)]
11. Han, F.; Salgado, R.; Prezzi, M.; Lim, J. Shaft and base resistance of non-displacement piles in sand. *Comput. Geotech.* **2017**, *83*, 184–197. [[CrossRef](#)]
12. Wu, W.; Lu, C.; Chen, L.; Mei, G.; El Naggar, M.H.; Liu, H. Horizontal vibration characteristics of pile groups in unsaturated soil considering coupled pile–pile interaction. *Ocean. Eng.* **2023**, *281*, 115000. [[CrossRef](#)]
13. Zhang, Y.; Di, T.; El Naggar, M.H.; Wu, W.; Liu, H.; Jiang, G. Modified Rayleigh-Love rod model for 3D dynamic analysis of large-diameter thin-walled pipe pile embedded in multilayered soils. *Comput. Geotech.* **2022**, *149*, 104853. [[CrossRef](#)]
14. Burland, J. *Shaft Friction of Piles in Clay—A Simple Fundamental Approach*; Ground Engineering: Brentwood, UK, 1973; Volume 6.
15. Kulhawy, F.H. Drilled shaft foundations. In *Foundation Engineering Handbook*; Springer: Boston, MA, USA, 1991.
16. Meyerhof, G.; Adams, J. The ultimate uplift capacity of foundations. *Can. Geotech. J.* **1968**, *5*, 225–244. [[CrossRef](#)]
17. API. *Recommended Practice for Planning, Designing, and Constructing Fixed Offshore Platforms*; American Petroleum Institute: Washington, DC, USA, 1989.
18. Toolan, F.; Lings, M.; Mirza, U. An appraisal of API RP2A recommendations for determining skin friction of piles in sand. In Proceedings of the Offshore Technology Conference, Houston, TX, USA, 7–10 May 1990.
19. Randolph, M.; Dolwin, R.; Beck, R. Design of driven piles in sand. *Géotechnique* **1994**, *44*, 427–448. [[CrossRef](#)]
20. Jardine, R.J.; Standing, J.R.; Chow, F.C. Some observations of the effects of time on the capacity of piles driven in sand. *Géotechnique* **2006**, *56*, 227–244. [[CrossRef](#)]
21. Jazebi, M.; Ahmadi, M.M. A numerical approach on side resistance of drilled shafts embedded in sandy soils. *Int. J. Geotech. Eng.* **2020**, *14*, 644–652. [[CrossRef](#)]
22. Potyondy, J.G. Skin friction between various soils and construction materials. *Géotechnique* **1961**, *11*, 339–353. [[CrossRef](#)]
23. Coyle, H.M.; Sulaiman, I.H. Skin friction for steel piles in sand. *J. Soil Mech. Found. Div.* **1967**, *93*, 261–278. [[CrossRef](#)]
24. Kulhawy, F.; Peterson, M. Behavior of sand-concrete interfaces. In Proceedings of the 6th Panamerican Conference on Soil Mechanics and Geotechnical Engineering, Lima, Peru, 2–7 December 1979; pp. 225–236.
25. Yoshimi, Y.; Kishida, T. A ring torsion apparatus for evaluating friction between soil and metal surfaces. *Geotech. Test. J.* **1981**, *4*, 145–152. [[CrossRef](#)]
26. Acar, Y.B.; Durgunoglu, H.T.; Tumay, M.T. Interface properties of sand. *J. Geotech. Geoenviron. Eng.* **1982**, *108*, 648–654. [[CrossRef](#)]
27. Uesugi, M.; Kishida, H. Influential factors of friction between steel and dry sands. *Soil Found.* **1986**, *26*, 33–46. [[CrossRef](#)] [[PubMed](#)]
28. Bosscher, P.J.; Ortiz, G.C. Frictional properties between sand and various construction materials. *J. Geotech. Eng.* **1987**, *113*, 1035–1039. [[CrossRef](#)]
29. Subba RAO, K.; Rao, K.; Allam, M.; Robinson, R. Interfacial friction between sands and solid surfaces. *Proc. Inst. Civ. Eng. Geotech. Eng.* **1998**, *131*, 75–82. [[CrossRef](#)]
30. Reddy, E.S.; Chapman, D.; Sastry, V. Direct shear interface test for shaft capacity of piles in sand. *Geotech. Test. J.* **2000**, *23*, 199–205.
31. Tiwari, B.; Ajmera, B.; Kaya, G. Shear strength reduction at soil structure interface. In *GeoFlorida 2010: Advances in Analysis, Modeling Design*; American Society of Civil Engineers: Reston, VA, USA, 2010.

32. Aksoy, H.S.; Gor, M.; Inal, E. A new design chart for estimating friction angle between soil and pile materials. *Geomech. Eng.* **2016**, *10*, 315–324. [[CrossRef](#)]
33. Han, F.; Ganju, E.; Salgado, R.; Prezzi, M. Effects of interface roughness, particle geometry, and gradation on the sand–steel interface friction angle. *J. Geotech. Geoenviron. Eng.* **2018**, *144*, 04018096. [[CrossRef](#)]
34. Wu, W.; Wang, Z.; Zhang, Y.; El Naggar, M.H.; Wu, T.; Wen, M. Semi-analytical solution for negative skin friction development on deep foundations in coastal reclamation areas. *Int. J. Mech. Sci.* **2023**, *241*, 107981. [[CrossRef](#)]
35. Zhang, Y.; El Naggar, M.H.; Wu, W.; Wang, Z.; Yang, X.; Jiang, G. Dynamic torsional impedance of large-diameter pipe pile for offshore engineering: 3D analytical solution. *Appl. Math. Model.* **2022**, *111*, 664–680. [[CrossRef](#)]
36. Wu, W.; Zhang, Y. A review of pile foundations in viscoelastic medium: Dynamic analysis and wave propagation modeling. *Energies* **2022**, *15*, 9432. [[CrossRef](#)]
37. Alawneh, A. Tension piles in sand: A method including degradation of shaft friction during pile driving. *Transp. Res. Rec.* **1999**, *1663*, 41–49. [[CrossRef](#)]
38. Gavin, K.G.; Lehane, B.M. The shaft capacity of pipe piles in sand. *Can. Geotech. J.* **2003**, *40*, 36–45. [[CrossRef](#)]
39. Rollins, K.M.; Clayton, R.J.; Mikesell, R.C.; Blaise, B.C. Drilled shaft side friction in gravelly soils. *J. Geotech. Geoenviron. Eng.* **2005**, *131*, 987–1003. [[CrossRef](#)]
40. Fioravante, V. On the shaft friction modelling of non-displacement piles in sand. *Soils Found.* **2002**, *42*, 23–33. [[CrossRef](#)]
41. Akgüner, C.; Kirkit, M. Axial bearing capacity of socketed single cast-in-place piles. *Soils Found.* **2012**, *52*, 59–68. [[CrossRef](#)]
42. Niazi, F.S.; Mayne, P.W. Cone penetration test based direct methods for evaluating static axial capacity of single piles. *Geotech. Geol. Eng.* **2013**, *31*, 979–1009. [[CrossRef](#)]
43. Tehrani, F.; Han, F.; Salgado, R.; Prezzi, M.; Tovar, R.; Castro, A. Effect of surface roughness on the shaft resistance of non-displacement piles embedded in sand. *Géotechnique* **2016**, *66*, 386–400. [[CrossRef](#)]
44. Tovar-Valencia, R.D.; Galvis-Castro, A.; Salgado, R.; Prezzi, M. Effect of surface roughness on the shaft resistance of displacement model piles in sand. *J. Geotech. Geoenviron. Eng.* **2018**, *144*, 04017120. [[CrossRef](#)]
45. Salgado, R.; Han, F.; Prezzi, M. Axial resistance of non-displacement piles and pile groups in sand. *Riv. Ital. Geotec.* **2017**, *51*, 35–46.
46. Rao, K.S.S.; Venkatesh, K. Uplift behaviour of short piles in uniform sand. *Soils Found.* **1985**, *25*, 1–7.
47. Azzam, W.R.; Al Mesmary, M. The behavior of single tension pile subjected to surcharge loading. *NED Univ. J. Res* **2010**, *7*, 1–12.
48. Ibrahim, S.F.; Hasan, H.F.; Fadhil, A.I. Evaluation of Bearing Capacity For Model Piles Driven In Sandy Soil. *J. Eng. Sustain. Dev.* **2014**, *18*, 28–54.
49. Emirler, B.; Tolun, M.; Yildiz, A. Investigation on determining uplift capacity and failure mechanism of the pile groups in sand. *Ocean. Eng.* **2020**, *218*, 108145. [[CrossRef](#)]
50. ASTM-C1444-00; Standard Method for Measuring the Angle of Repose of Free-Flowing Mold Powders. Method C1444-00. Annual Book of ASTM Standards; American Society of Testing and Materials: Philadelphia, PA, USA, 2001; pp. 694–695.
51. ASTM D422-63; Standard Test Method for Particle-Size Analysis of Soils. ASTM International: West Conshohocken PA, USA, 2007.
52. ASTM D854-14; Standard Test Methods for Specific Gravity of Soil Solids by Water Pycnometer. ASTM International: West Conshohocken, PA, USA, 2014.
53. ASTM D4254; Standard Test Methods for Minimum Index Density and Unit Weight of Soils and Calculation of Relative Density. ASTM International: West Conshohocken, PA, USA, 2006.
54. Bagriacik, B.; Laman, M. Distribution of Stresses in Unreinforced and Reinforced Soils Induced by a Circular Foundation. *J. Fac. Eng. Archit. Gazi Univ.* **2011**, *26*, 787–800.
55. Gandhi, S.R.; Selvam, S. Group Effect on Driven Piles under Lateral Load. *J. Geotech. Geoenviron. Eng.* **1997**, *123*, 702–709. [[CrossRef](#)]
56. Sawwaf, M. El, Experimental Study of Eccentrically Loaded Raft with Connected and Unconnected Short Piles. *J. Geotech. Geoenviron. Eng.* **2010**, *136*, 1394–1402. [[CrossRef](#)]
57. Wood, D.M. *Geotechnical Modelling (Applied Geotechnics; v. 1)*; Taylor & Francis Group/Books: Boca Raton, FL, USA, 2004.
58. Abdulla, N.A. Concrete filled PVC tube: A review. *Constr. Build. Mater.* **2017**, *156*, 321–329. [[CrossRef](#)]
59. Ayanleye, S.; Udele, K.; Nasir, V.; Zhang, X.; Miltz, H. Durability and protection of mass timber structures: A review. *J. Build. Eng.* **2022**, *46*, 103731. [[CrossRef](#)]
60. Wu, J.; Zhu, Y.; Li, C. Experimental Investigation of Fatigue Capacity of Bending-Anchored CFRP Cables. *Polymers* **2023**, *15*, 2483. [[CrossRef](#)]
61. Chen, T.-J.; Fang, Y.-S. Earth pressure due to vibratory compaction. *J. Geotech. Geoenviron. Eng.* **2008**, *134*, 437–444. [[CrossRef](#)]
62. El Sawwaf, M.; Nazir, A.K. Behavior of repeatedly loaded rectangular footings resting on reinforced sand. *Alex. Eng. J.* **2010**, *49*, 349–356. [[CrossRef](#)]
63. ASTM D-3080; Standard Test Method for Direct Shear Test of Soils under Consolidated Drained Conditions. ASTM International: West Conshohocken, PA, USA, 2011.
64. ASTM D5321/D5321M-17; Standard Test Method for Determining the Shear Strength of Soil-Geosynthetic and Geosynthetic-Geosynthetic Interfaces by Direct Shear. ASTM International: West Conshohocken, PA, USA, 2017.

65. Pando, M.A.; Filz, G.M.; Dove, J.E.; Hoppe, E.J. Interface shear tests on FRP composite piles. In *Deep Foundations 2002: An International Perspective on Theory, Design, Construction, and Performance*; American Society of Civil Engineers: Reston, VA, USA, 2002.
66. Stark, N.; Hay, A.; Cheel, R.; Lake, C. The impact of particle shape on the angle of internal friction and the implications for sediment dynamics at a steep, mixed sand–gravel beach. *Earth Surf. Dyn.* **2014**, *2*, 469–480. [[CrossRef](#)]
67. Mullins, G.; Winters, D.; Dapp, S. Predicting end bearing capacity of post-grouted drilled shaft in cohesionless soils. *J. Geotech. Geoenviron. Eng.* **2006**, *132*, 478–487. [[CrossRef](#)]
68. Al-Mhaidib, A.I. Shearing rate effect on interfacial friction between sand and steel. In Proceedings of the Fifteenth International Offshore and Polar Engineering Conference, Seoul, Republic of Korea, 19–24 June 2005.
69. Hettler, A. Approximation Formulae for Piles under Tension. 1982. Available online: <https://pascal-francis.inist.fr/vibad/index.php?action=getRecordDetail&idt=PASCALGEODEBRGM8320254224> (accessed on 8 August 2022).
70. Alawneh, A.S.; Malkawi, A.I.H.; Al-Deeky, H. Tension tests on smooth and rough model piles in dry sand. *Can. Geotech. J.* **1999**, *36*, 746–753. [[CrossRef](#)]

**Disclaimer/Publisher’s Note:** The statements, opinions and data contained in all publications are solely those of the individual author(s) and contributor(s) and not of MDPI and/or the editor(s). MDPI and/or the editor(s) disclaim responsibility for any injury to people or property resulting from any ideas, methods, instructions or products referred to in the content.